Electronic Supplementary Material (ESI) for Energy & Environmental Science.
This journal is © The Royal Society of Chemistry 2019

Electronic Supplementary Information

Energy scavenging from ultra-low temperature gradients

Ravi Anant Kishore,*[a] Brent Davis,[a] Jake Greathouse,[a] Austin Hannon,[a] David Kennedy,[a] Alec Millar,[a] Danny Mittel,[a] Amin Nozariasbmarz,[b] Min Gyu Kang,[a] Han-Byul Kang,[a] Mohan Sanghadasa [c] and Shashank Priya*[a,b]

[a] Center for Energy Harvesting Materials and Systems (CEHMS), Virginia Tech, Blacksburg, VA 24061, USA.

[b] Department of Materials Science and Engineering, Pennsylvania State University, University Park, PA 16802, USA.

[c] Aviation and Missile Research, Development, and Engineering Center, US Army RDECOM, Redstone Arsenal, AL 35898, USA.

Thermomagnetic effect

The change in magnetic properties of a certain material in response to its changing thermal environment is termed as thermomagnetic effect (TME). TME is prominent in the ferromagnetic materials and it has been found to be significant when the cyclic variation in the temperature occurs across the Curie point in presence of a varying external magnetic field.[1-3] Curie point is defined as a temperature where a thermomagnetic material undergoes phase transition from a highly magnetic state to a weakly magnetic state in a narrow temperature range, losing its spontaneous magnetization. The concept of converting heat into mechanical or electrical work using TME was first introduced in late 19th century,[4-7] but the performance of these thermomagnetic devices was

too poor to be cost-effective. The problem lies with the ferromagnetic materials used in these devices. The conventional ferromagnetic materials such as iron, cobalt, and nickel have very high Curie temperature (~350-1100°C), which presents several implementation changes. Since the magnetic phase change occurs in a narrow temperature range, cyclic variation in temperature (ΔT) is small. Consequently, the Carnot efficiency, $\frac{\Delta T}{T_h}$, for the thermomagnetic heat engines utilizing the conventional ferromagnetic materials is quite poor, not more than few percent.[8] Gadolinium (Gd) having low Curie temperature ~22°C (i.e. near room temperature) has been suggested as a better thermomagnetic material for thermal energy harvesting than the conventional ferromagnetic materials. Under same value of ΔT, Gd is expected to exhibit relatively higher Carnot efficiency than the conventional ferromagnetic materials. In recent years, several other materials, such as $Gd_5(Si_2Ge_2)$, Heusler alloys, MnAs and its related compounds, and lanthanide transition-metal-based compounds have been prepared in laboratory and are claimed to exhibit 2 to 10 times higher thermomagnetic effect than Gd.[8, 9] For thermal energy harvesting, however, along with high thermomagnetic response, the working material needs to have the following features:[9]

(i) Curie temperature near and above the room temperature so that ambient can be used as the heat sink;

(ii) minimal thermal and magnetic hysteresis to maximize work output per thermomagnetic cycle;

(iii) high thermal conductivity and low heat capacity to ensure effective heat transfer and rapid temperature change;

(iv) large electric resistance to minimize the eddy current losses;

(v) good mechanical strength, stability, and machinability for device manufacturing;

(vi) Cost-effective.

Most thermomagnetic materials that exhibit giant thermomagnetic effect undergo first-order phase change, which is often accompanied by large thermal hysteresis.[10] Moreover, thermal and mechanical properties of these prototype materials are not readily available in literature. In this study, therefore, we have employed the most established and widely used thermomagnetic material, Gd, as our working material and we believe that the performance of the PoWER devices can be improved in near future by utilizing a better thermomagnetic material.

Thermomagnetic cycle

An ideal thermomagnetic cycle is shown in Fig. S1a, where a thermomagnetic material, such as a portion of the PoWER rotor, undergoes ferromagnetic ↔ paramagnetic phase transition in a cyclic manner. In Fig S1, state 1 represents initial condition of the thermomagnetic material, where it is below its Curie temperature and ferromagnetic. During process 1-2, a strong external magnetic field is applied while the temperature is maintained constant (isothermal process). The material is then heated during process 2-3, while the applied magnetic field is held constant (isofield heating). Later during process 3-4, the applied magnetic field is slowly removed, while the material is still hot (isothermal process). Lastly, when the external magnetic field is near zero, the material is cooled during process 4-1 (isofield cooling).

Magnetic work per thermodynamic cycle is represented by the enclosed area 1-2-3-4 as shown in Fig. S1a and, mathematically, it is expressed as:

$$w_{out} = \oint \mu_o H dM \tag{S1}$$

where dM denotes the infinitesimal change in magnetization under the applied external magnetic field $\mu_o H$. The thermomagnetic cycle can also be presented using temperature-entropy (T-s) diagram as shown in Fig. S1b. The shaded region 1-2-3-4 represents the magnetic work per thermodynamic cycle and it is mathematically given as:

$$w_{out} = \oint T ds \tag{S2}$$

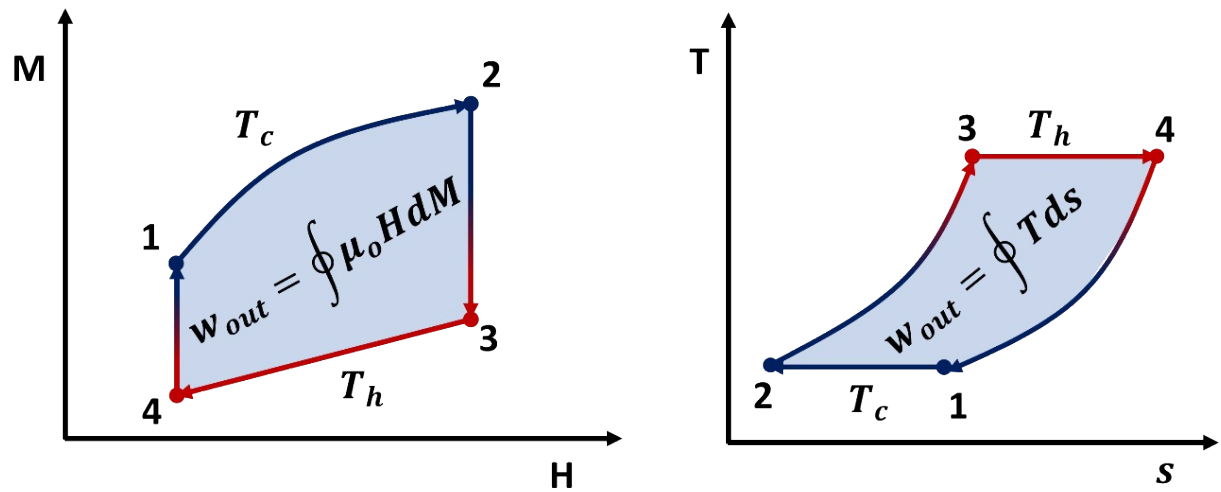

Fig. S1. An ideal thermomagnetic cycle. A thermomagnetic material undergoes ferromagnetic ↔ paramagnetic phase change in a cyclic manner. (a) The enclosed area 1-2-3-4 in the M-H diagram represents the specific magnetic work (work per unit mass of the thermomagnetic material) per thermomagnetic cycle. (b) The thermomagnetic cycle on temperature-entropy (T-s) diagram.

In order to determine the efficiency of the thermomagnetic cycle, the heat inflow, q_{in} needs to be determined. The heat inflow q_{in} can be given as:

$$q_{in} = \int_{2}^{3} T\, ds + \int_{3}^{4} T\, ds \tag{S3}$$

The entropy of a ferromagnet is a function of temperature (T) and magnetic field (μ_oH), i.e. $s = s(T, \mu_o H)$. Therefore, change in the specific entropy can be expressed as:[9]

$$ds = \left(\frac{\partial s}{\partial T}\right)_{\mu_o H} dT + \left(\frac{\partial s}{\partial H}\right)_T dH \tag{S4}$$

The first partial derivative, $\left(\frac{\partial s}{\partial T}\right)_{\mu_o H}$ can be defined in terms of specific heat capacity (C_H) at constant magnetic field as:[9]

$$C_H(\mu_o H, T) = T\left(\frac{\partial s}{\partial T}\right)_{\mu_o H} \tag{S5}$$

The second term $\left(\frac{\partial s}{\partial H}\right)_T$ denotes change in entropy due to change in magnetic field at constant temperature and it is termed as change in the magnetic entropy (δs_m). Using Equations (S4)-(S5), Equation (S3) can be expressed as:

$$q_{in} = \int_{2}^{3} C_H dT + \int_{2}^{3} T\, ds_m + \int_{3}^{4} T\, ds_m \tag{S6}$$

Similarly, the heat outflow q_{out} during cooling process can be expressed as:

$$q_{out} = \int_4^1 C_H dT + \int_4^1 T\, ds_m + \int_1^2 T\, ds_m \tag{S7}$$

When the applied magnetic fields is small ($< 2T$), the term $\int_4^1 T\, ds_m + \int_1^2 T\, ds_m$ has been found to be negligible in comparison to the first term $\int_4^1 C_H dT$.[11] The efficiency of the thermomagnetic cycle can be expressed as:

$$\eta = \frac{w_{out}}{q_{in}} = \frac{w_{out}}{q_{out} + w_{out}} \approx \frac{\oint \mu_o H dM}{\int_{T_c}^{T_h} C_{H=0} dT + \oint \mu_o H dM} \approx \frac{\oint \mu_o H dM}{\int_{T_c}^{T_h} C_{H=0} dT} \tag{S8}$$

Temperature sweep experiment for a PoWER device with two rotors

Fig. S2 and S3 depict the temperature sweep experiment for the PoWER device with two rotors. As indicated in Fig. S2, the rotor rpm initially increases with increase in water temperature, attains a maximum value at 30-35°C, and then slowly decreases with further increase in temperature. A similar trend can be observed for power-temperature plot in Fig. S3. The electrical power of the PoWER device increases with increase in temperature, reaches a maximum value at around 30-40°C, and then decreases slowly.

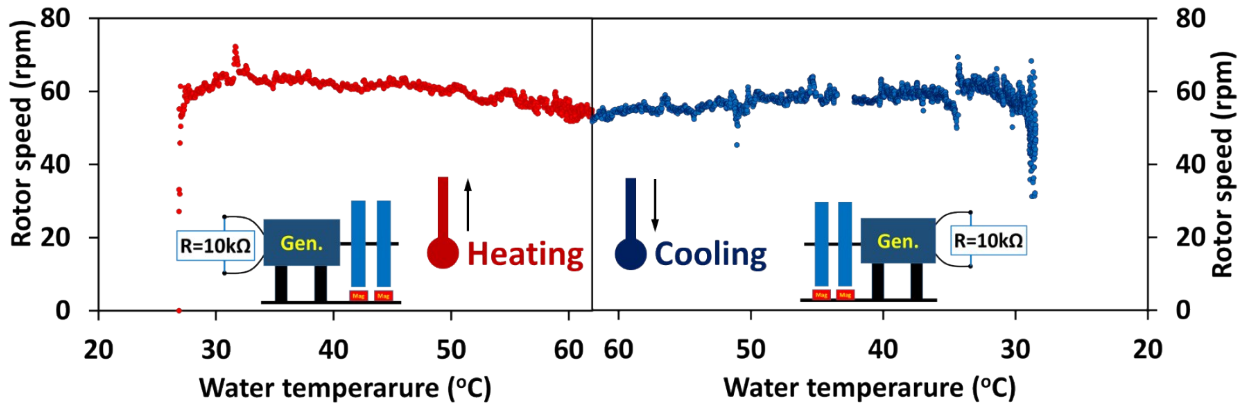

Fig. S2. Temperature sweep experiment for the PoWER device with two rotors. Angular speed of the rotor first increases with increase in temperature, reaches a maximum value at 30-40°C, and then decreases slowly.

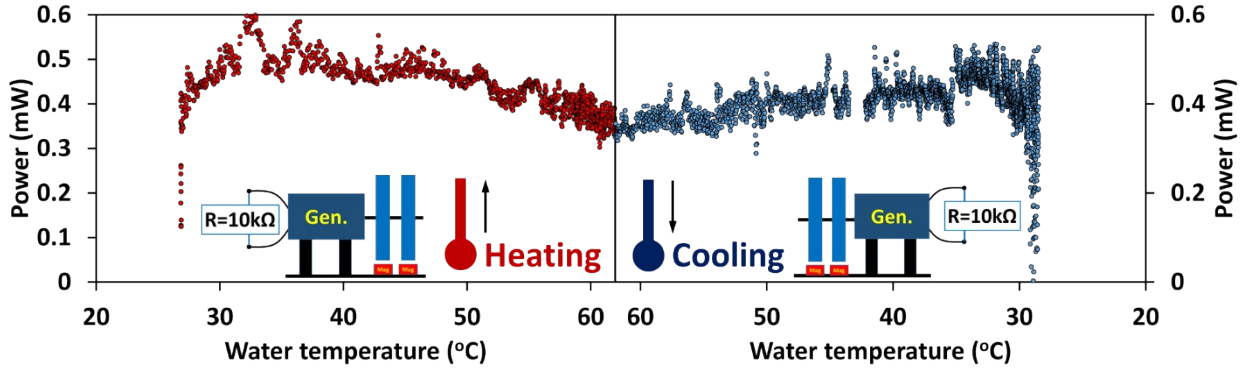

Fig. S3. Power-temperature plot for the PoWER device with two rotors. The electrical power initially enhances with an increase in temperature, reaches a maximum value at 30-40°C, and then decreases slowly.

Scalability of PoWER devices

Fig. S4a and b compare the electrical power generated by PoWER devices having different size of rotors. The PoWER device used in Fig. S4a comprises of two rotors with outer dimeter of 25.5 mm, inner diameter of 19.5 mm and thickness of 1.5 mm; whereas, the PoWER device used in Fig. S4b comprises of one rotor of outer dimeter of 50.5 mm, inner diameter of 44.5 mm and thickness of 1.5 mm. It can be noted that increasing the size of the rotor positively impacts the performance of PoWER devices due to the increased thermal gradient. The optimal average electrical power increased from 0.204 mW to 0.385 mW by increasing the outer diameter of the rotor from 25.5 mm to 50.5 mm.

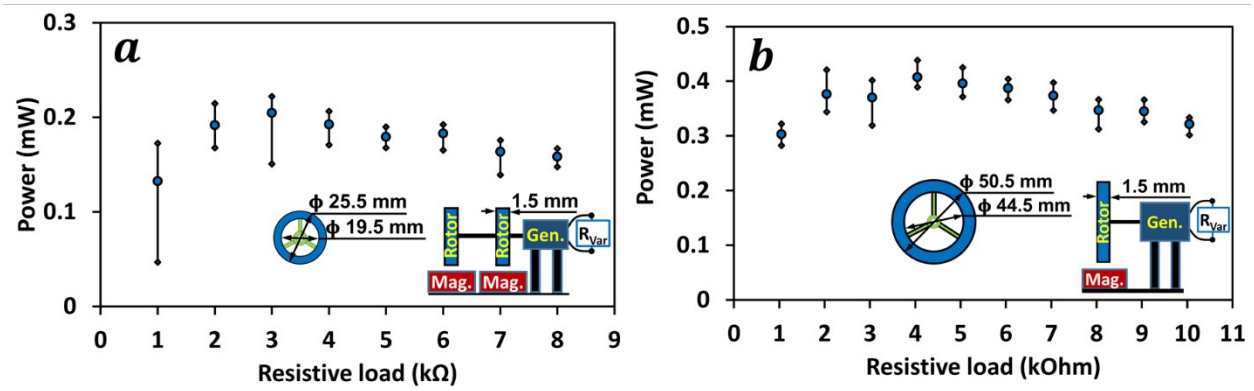

Fig. S4. The effect of rotor size on the performance of PoWER devices. (a) Electrical power generated by PoWER devices having rotor of dimensions (a) 25.5 mm (OD), 19.5 mm (ID), and 1.5 mm (thickness) and (b) 50.5 mm (OD), 44.5 mm (ID), and 1.5 mm (thickness). Increasing the size of the rotor positively influences the performance of PoWER devices due to increased thermal gradient.

The generated electrical power can also be increased by connecting several PoWER devices. Mechanical to electrical energy conversion in an electrical generator is usually accompanied by various kind of losses, such as copper loss, hysteresis loss, eddy current loss, and mechanical loss. The generator losses can be minimized by attaching several rotors to a single electrical generator. Fig. S5 illustrates the electrical power generated by PoWER devices having variable number of rotors connected in series to an electrical generator. Fig. S5a illustrates the electrical power when water temperature is 32°C, while Fig. S5b illustrates the electrical power when water temperature is 40°C. Increasing the number of rotors in series from 1 to 6 increases electrical power from 0.31 mW to 1.10 mW (3.6 times) at 32°C and from 0.30 mW to 1.30 mW (4.5 times) at 40°C. As illustrated in Fig. 4c in the manuscript, the optimal power of the PoWER device increases almost linearly with increase in the number of rotors.

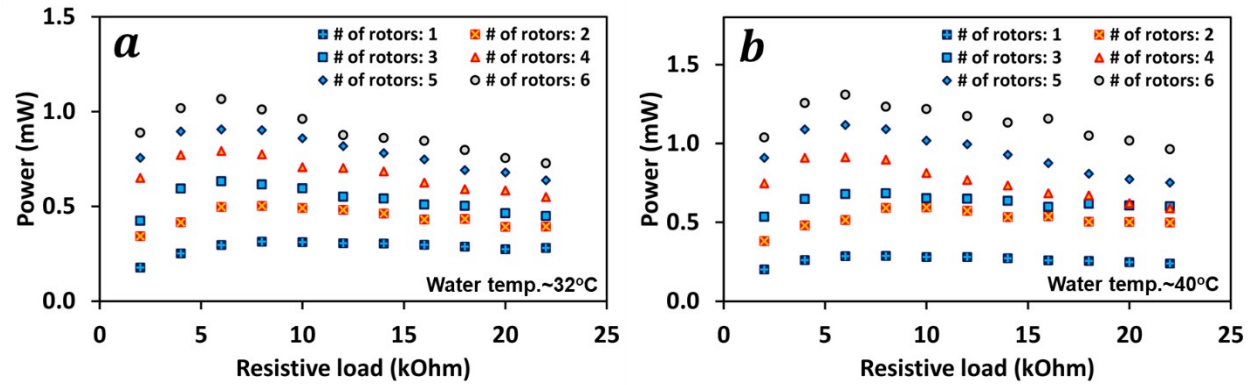

Fig. S5. The electrical power generated by PoWER devices having variable number of rotors connected in series to an electrical generator. Increasing the number of rotors in series from 1 to 6 increases electrical power by (a) 3.6 times at 32°C and (b) 4.5 times at 40°C.

Axial flux generator

The commercial electric generators are typically designed for high shaft speed (> 1000 rpm). The PoWER devices operate at very low angular speed (less than 220 rpm). Also, the magnetic torque of the PoWER rotor was calculated to be very small (less than 1.0 mN-m). Therefore, none of the commercial generator, available off-the-shelf, were found to be suitable for the PoWER devices. We fabricated an indigenous axial flux generator, which consists of one stator and two rotors (Fig. S6). The generator stator has eight copper wire coils. The teardrop shape of the coil, shown is Fig. S6a, was designed to match the shape of the magnetic field distribution in order to maximize the mechanical to electrical energy conversion thereby increasing the overall conversion efficiency. Each of the generator rotors contains eight arc shaped neodymium magnets (Fig. S6c). These permanent magnets are arranged in a circular manner and in the alternate polarity. The generator that was used with the PoWER device with single rotor has diameter of 30 mm and each coil contains about 900 turns. The neodymium magnets have outside diameter (OD) of 23.5 mm, inside diameter (ID) of 11.0 mm, and arc angle of 42°. The PoWER device with variable number of rotors required a slightly bigger generator of diameter 34 mm. The coils contain 1300 turns of 42 AWG copper wire. The arc-shaped neodymium magnets have dimension: 30.0 mm (OD), 12.5 mm (ID), and arc angle of 42°.

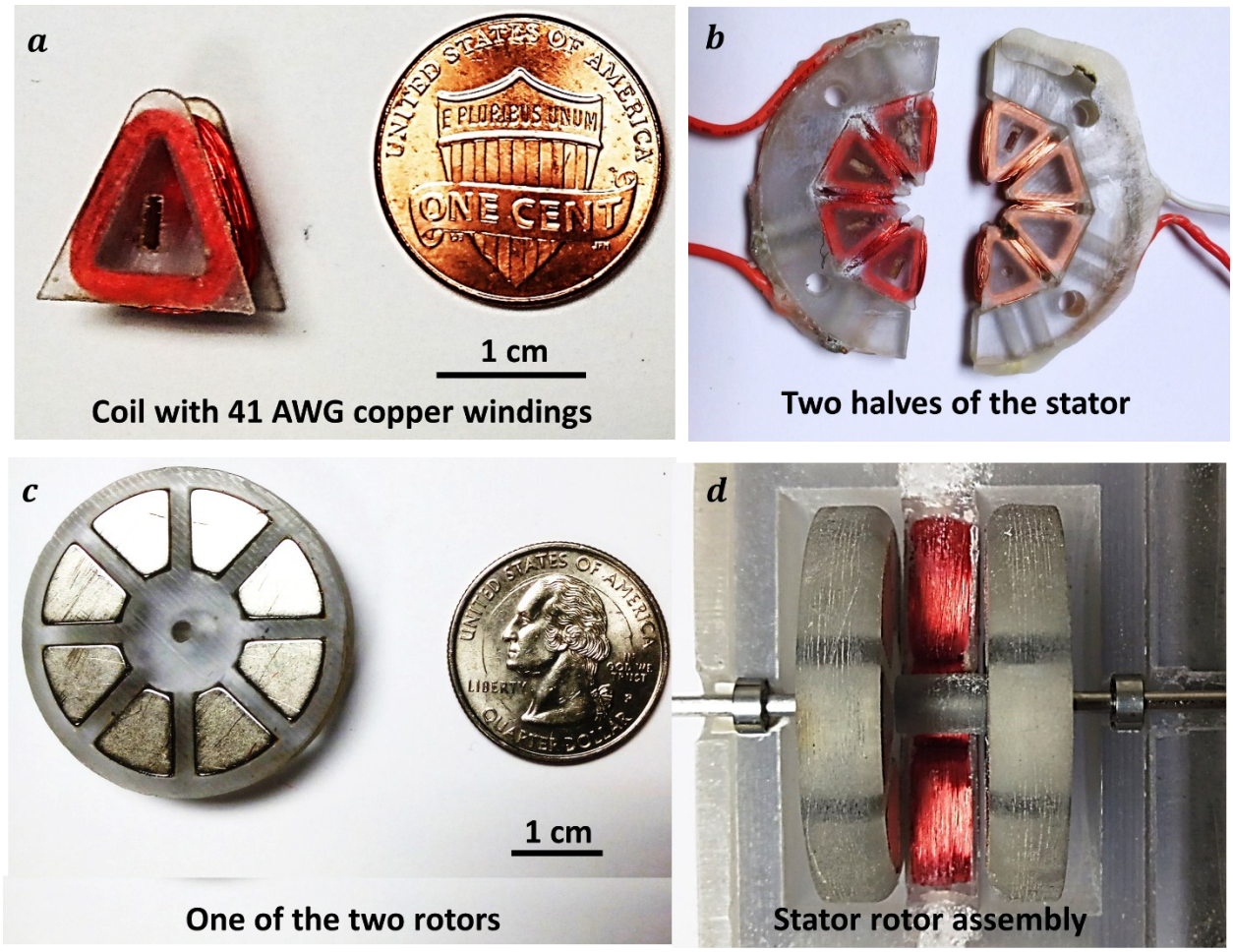

Fig. S6. Axial flux generator used in the PoWER devices. (a) The teardrop shaped layout of the generator's coil. (b) Two halves of the generator stator, containing four coils each. (c) One of the two rotors of the generator. (d) Stator-rotor assembly (only one half of the stator is shown).

Fig. S7 shows the variation in the magnetic flux density generated by the generator's rotor versus distance. The magnetic flux density reduces to ~100 Gauss after a distance of 10 mm. In all the experimental prototypes, the rotor closest to the generator was placed more than 15 mm away, indicating no substantial interaction between the rotors and the generator.

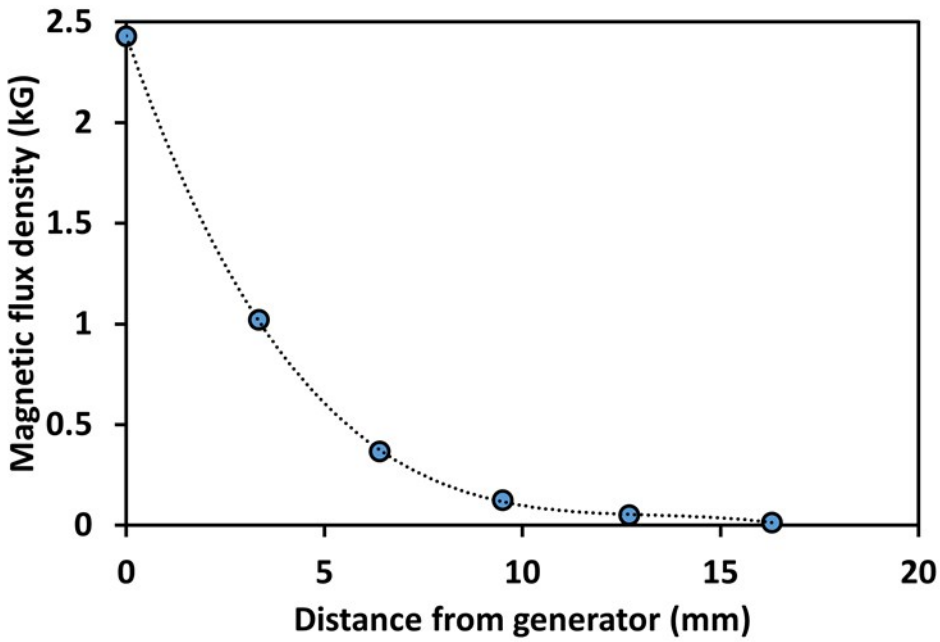

Fig. S7. Variation in the magnetic flux density generated by the generator's rotor versus distance.

Predicting PoWER performance using numerical model

In order to describe the behavior of the PoWER device using mathematical models, we require advanced mathematics to couple multiple physics: heat transfer, fluid flow, magnetism, and mechanics. We need to simultaneously solve Maxwell's equations for electromagnetic analysis, Navier-Stokes equations for fluid flow, and thermal transport equations for heat transfer analysis, subject to appropriate boundary conditions. Since all three physics are directly coupled, finding an analytical solution is cumbersome. In this study, we employed commercial code, COMSOL Multiphysics, version 5.3 (COMSOL, Inc. USA) to numerically solve this multi-physics problem.

Each of these physics is briefly described below.

Magnetostatics equation

The equation of magnetostatics is expressed as: [12]

$$\nabla \times \left(\mu_o^{-1} \nabla \times A - M\right) - \sigma\, v \times (\nabla\, x\, A) = J_e \tag{S9}$$

where μ_0 is the permeability of vacuum and σ is the electrical conductivity, v denotes the velocity of the conductor, J_e is the externally generated current density, **A** is magnetic vector potential and **M** is magnetization vector.

Fluid flow equation

Since the temperature variations are small, the working fluids (air and water) have been assumed to be incompressible. In addition, since the Reynolds number was found to be less than 1500 for air and less than 10 for water, the fluid flows have been considered laminar. The Navier-Stokes equations for an incompressible laminar flow are given as:[12]

$$\rho \nabla \cdot u = 0 \tag{S10}$$

$$\rho \frac{\partial u}{\partial t} + \rho (u.\nabla) u = \nabla \cdot \left[-pI + \mu\left(\nabla u + (\nabla u)^T\right)\right] + F \tag{S11}$$

where ρ is the fluid density, **u** is the velocity vector, p is pressure, and **F** is the volume force vector.

Heat diffusion equation

The heat transfer in solids is described by heat diffusion equation, which is given as:[12]

$$\rho C_p \frac{\partial T}{\partial t} - \nabla \cdot (\kappa \nabla T) = Q \tag{S12}$$

where T is temperature, ρ is density, C_p is heat capacity at constant pressure, and κ is thermal conductivity of the material. Term Q on the right represents the collective heat flow from various

heat sources (or sinks). In this study, since the rotor is moving, we need to add an additional term to account for the rotor movement. Equation (S12) now modifies to:[12]

$$\rho C_p \frac{\partial T}{\partial t} - \nabla \cdot (k \nabla T) + \rho C_p u \cdot \nabla T = Q \tag{S13}$$

Thermal transport equation for the fluid contains addition terms for the pressure work and viscous heating and it is given as:[12]

$$\rho C_p \left(\frac{\partial T}{\partial t} + (u \cdot \nabla) T \right) = - (\nabla \cdot q) + \tau : S - \frac{T}{\rho} \left(\frac{\partial \rho}{\partial T} \right)_p \left(\frac{\partial p}{\partial t} + (u \cdot \nabla) p \right) + Q \tag{S14}$$

where q is the heat flux by conduction, p is pressure, τ is the viscous stress tensor, and S is the strain-rate tensor. In this study, since the involved fluids are water and air and device dimension is small, heating contribution by pressure and viscosity terms has been ignored.

Boundary conditions

The residual flux density of N42 Neodymium Magnet typically lies in the range of 1.30-1.32 T. In this study, we have considered the remanent magnetic flux density of the permanent magnets as 1.32 T. The exterior boundaries of air domain are assigned 'Perfect Magnetic Conductor' that represents the boundary where the tangential magnetic field vanishes to zero. Mathematically, it is given as:[12]

$$n \times H = 0 \tag{S15}$$

where n is the normal vector of the boundary.

The bottom of water reservoir is given a constant hot-side temperature boundary condition of 40°C. The boundaries of the air domain are defined as 'open boundaries' fixed at temperature of 22°C. Open boundaries in COMSOL heat-transfer interface follows the following conditions:[12]

$$T = T_{\infty}, \text{ if } n \cdot u < 0$$

$$-n \cdot q = 0, \text{ if } n \cdot u \geq 0 \tag{S16}$$

where T_{∞} is the specified ambient temperature, i.e. 22°C.

We assigned 'no-slip' wall boundary condition at the boundaries of the water domain touching the permanent magnet and the container. Since the permanent magnet and container are stationary, this leads to zero velocity at these boundaries.[12]

$$u = 0 \tag{S17}$$

The water boundary touching the rotor was assigned as 'sliding wall' boundary condition. The velocity of the tangentially moving wall was given as:[12]

$$U_w = r\omega \tag{S18}$$

where ω is the angular speed of the rotor and r denotes its outer radius.

Since the numerical model considered in this study is two dimensional, we need to define appropriate boundary conditions to account for out-of-plane heat flux. The total heat flux through the two side surfaces of the rotor is given as:[12]

$$q = h_{\infty}(T - T_{\infty}) \tag{S19}$$

Based on the results reported by Elghnam [13] for a rotating cylinder in air, we estimated the heat transfer coefficient, $h_{a,\infty}$, to be around 14 W/m^2-K. For the small side portion of the rotor touching the hot water, we have assumed heat transfer coefficient, $h_{w,\infty}$, of 100 W/m^2-K.

Effect of number of permanent magnets

Fig. S8a illustrates 2-magnet and 1-magnet configurations. As shown, 1-magnet configuration contains only one permanent magnet, which is placed on one side of the PoWER rotor. 2-magnet configuration, on the other hand, consists of two permanent magnets, which are placed in the opposite polarity on the two sides of the PoWER rotor. Fig. S8b shows the arrows indicating magnetization on the rotor surface in the two magnetic configurations. It can be noted that 1-magnet configuration exerts only a push force on the rotor, whereas 2-magnet configuration exerts both push as well as push magnetic forces on the rotor. Fig. S8c and d compare the rotor speed and the magnetic torque in the two cases. It can be observed that 1-magnet configuration generates an unbalanced torque on the rotor from the beginning of the time that causes the rotor to rotate without any noticeable time lag. On the other hand, 2-magnet configuration provides a braking torque on the rotor in the beginning. This allows the PoWER rotor to achieve a larger thermal gradient. In addition, push and pull magnetic forces from the two sides result in a higher magnetic torque (Fig. S8d) and the higher angular speed (Fig. S8c) in 2-magnet configuration that in 1-magnet configuration. It can be seen that the maximum angular speed achieved by the rotor with two magnets is almost twice of the maximum angular speed gained by the rotor with one magnet. Clearly, 2-magnet configuration is a superior design; therefore, all the results presented on this paper were obtained for PoWER devices containing two permanent magnets.

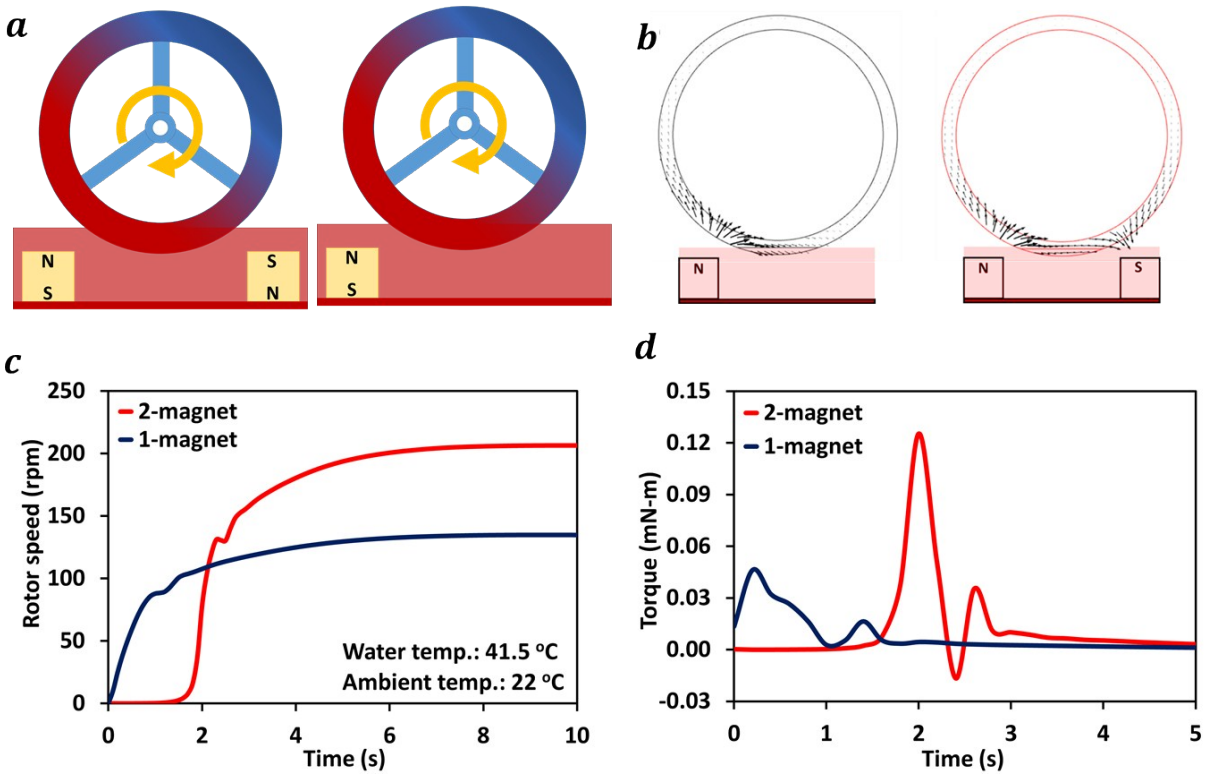

Fig. S8. Effect of number of permanent magnets on the performance of PoWER devices. (a) 1-magnet and 2-magnet configurations. (b) The arrows indicating magnetization on the rotor surface in the two magnetic configurations. (c) Variation of angular speed with time. (d) Variation of magnetic torque versus time. 2-magnet configuration is a superior design as it results in higher rpm as well higher magnetic torque.

Effect of magnetic field strength

Fig. S9 shows the effect of increasing remanent field intensity of the permanent magnets on the angular speed of the PoWER rotor. It can be noted that increasing remanent field intensity of the permanent magnets has positive effect on the angular speed of the rotor. When remanent field

intensity is increases from 0.7 T to 1.3 T (1.85 times), maximum angular speed of the rotor increases almost linearly from 120 rpm to 240 rad/s (2.0 times).

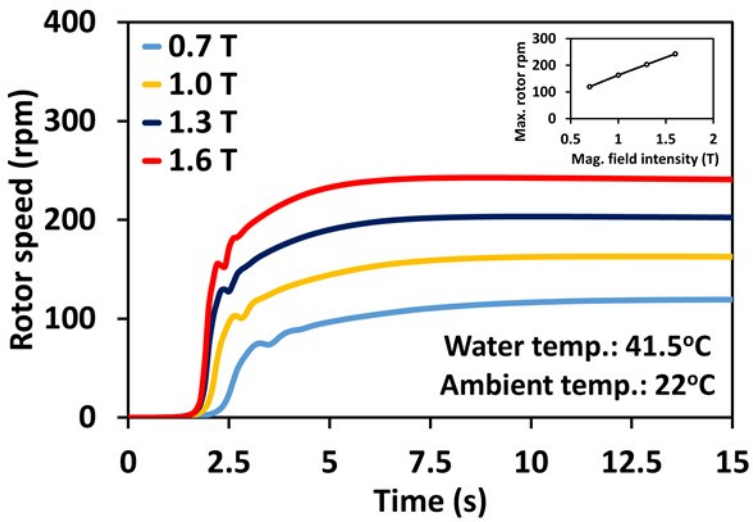

Fig. S9. Effect of magnetic field strength on the performance of the PoWER devices. Maximum rpm increases almost linearly with increase in remanent field intensity of the permanent magnets.

Effect of hot-side (water) temperature

Fig. S10 shows the variation in angular speed of the PoWER rotor versus time at different hot-side (water) temperature. The cold-side temperature is fixed at 22°C. The maximum angular speed of the rotor first increases with increase in water temperature, reaches an optimal value (at 40°C) and then decreases with further increases in water temperature. This results is in agreement with the experimental observations shown in Fig. 5 and Fig. S2.

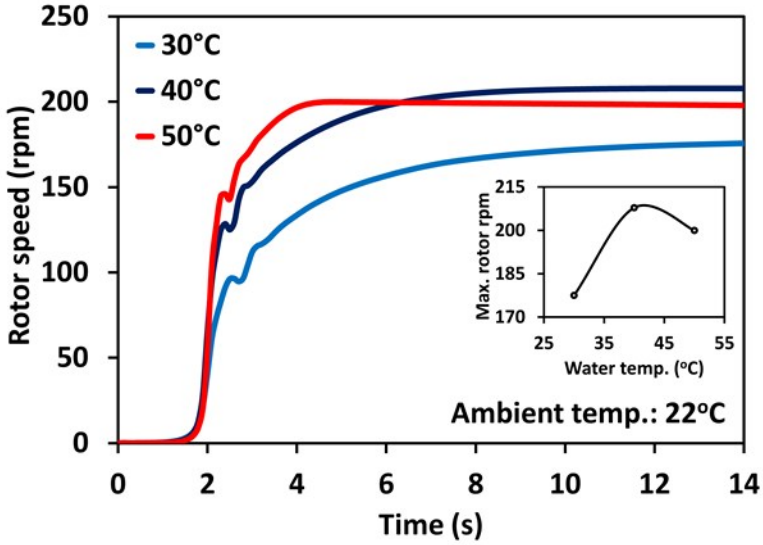

Fig. S10. Effect of hot-side (water) temperature on the performance of the PoWER devices.

Effect of cold-side (ambient) temperature

Fig. S11 shows the variation in rotor speed versus time at different cold-side (ambient) temperatures. The hot-side temperature is fixed at 41.5°C. It can be seen that the maximum angular speed of the rotor initially increases with decrease in the ambient temperature but it almost saturates below 12°C.

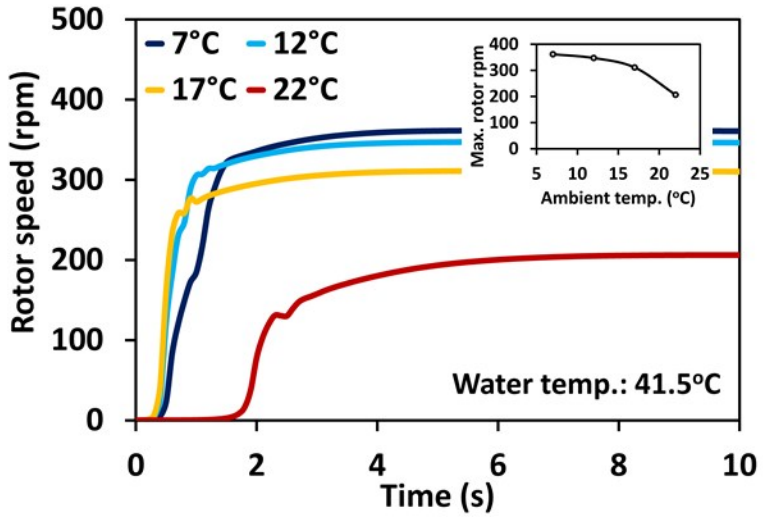

Fig. S11. Effect of cold-side (ambient) temperature on the performance of PoWER devices.

Supplementary videos

Video V1: The PoWER device operation in presence of no heat source but light wind of 1.5 m/s. The PoWER device does not self-start; however, once started manually, the rotor keeps oscillating and produces electric power.

Video V2: The PoWER device with a single rotor is kept on the surface of a laptop. Under temperature difference of just 3°C, the PoWER device can be seen to light up several LEDs.

Video V3: The operation of the PoWER device when it is located on sewer grill. The PoWER device can be used to generate electricity using the steam coming out of sewage and drainage system from industrial and commercial establishments.

Video V4: The PoWER device with a single rotor is kept on a metal bench exposed to sun light.

Video V5: A MIDASCON sensor being powered by the PoWER device. The sensor senses temperature, humidity, and acceleration and transmits the data wirelessly using Bluetooth.

Supplementary references

1. D. Solomon, *Journal of applied physics*, 1988, **63**, 915-921.
2. D. Solomon, *Journal of Applied Physics*, 1989, **65**, 3687-3693.
3. D. Solomon, *Energy Conversion and Management*, 1991, **31**, 157-173.
4. T. A. Edison, *US Pat., 380100*, 1888.
5. T. A. Edison, *US Pat., 476983*, 1892.

6. N. Tesla, *US Pat., 396121*, 1889.

7. N. Tesla, *US Pat., 428057*, 1890.

8. R. A. Kishore and S. Priya, *Renewable and Sustainable Energy Reviews*, 2018, **81**, 33-44.

9. R. A. Kishore and S. Priya, *Sustainable Energy & Fuels*, 2017, **1**, 1899-1908.

10. B. Yu, Q. Gao, B. Zhang, X. Meng and Z. Chen, *International Journal of Refrigeration*, 2003, **26**, 622-636.

11. C.-J. Hsu, S. M. Sandoval, K. P. Wetzlar and G. P. Carman, *Journal of Applied Physics*, 2011, **110**, 123923.

12. C. Multiphysics, *COMSOL, AB*, 2012, 39-40.

13. R. I. Elghnam, *Ain Shams Engineering Journal*, 2014, **5**, 177-185.